Journal of the Nigerian Association of Mathematical Physics
Volume 62, (October – Dec., 2021 Issue), pp79 – 88

INFLUENCE OF NONLINEAR THERMAL RADIATION ON REACTIVE MHD NANOFLUID FLOW OVER A THIN NEEDLE WITH SLIP EFFECT

*J.C. Ukaegbu[1], F.A. Amao[1], M.U. Faruq[2], U.D. Akpan[3] and T. A. Yusuf[1]**

[1]Department of Mathematics, Adeleke University, Ede Osun State, Nigeria.
[2]Computer Science Department, School of I.C.T Kwara State College of Arabic and Islamic Legal Studies, Ilorin, Kwara State, Nigeria
[3]Department of Mathematics, Akwa Ibom State University, Mkpat Enin, Nigeria

Abstract

The steady Thompson and Troian slip boundary flow in a magnetohydrodynamic fluid over a thin needle with nonlinear thermal radiation is examined. Additional effects added to the novelty of the mathematical model are the combined influences of homogeneous-heterogeneous (HH) reaction and thermophoresis. In order to reform the mathematical model to a physical problem, dimensionless variables were used. Solutions are found numerically with the engagement of the shooting method for dimensionless velocity, temperature, and homogeneous-heterogeneous reaction. The behavior of dimensionless governing variables on the velocity, temperature, skin friction coefficient, and local Nusselt number are illustrated via graphs. Furthermore, a comparison with a published article in a limiting case is made and an excellent consensus is accomplished. It is witnessed that the wall dragging force is damped as the slip and the critical shear rate parameters values augment.

***Keywords*:** Nonlinear thermal radiation; Heat source; a thin needle; Thompson and Troian slip boundary condition; Homogeneous-heterogeneous reactions

Introduction

Numerous investigators have been drawn to the area involving chemical reactions, some reactions require catalysts to manifest, and others may not. To portray chemically reacting models such as combustion and biochemical systems, the Homogenous-Heterogeneous (HH) reactions is been considered. Reactions that occur within the fluid (Homogenous) while those that take effect on the surface of the catalyst are Heterogeneous. Practical areas where the HH reaction can be seen are in the ignition, biochemical processes, food processing, water, and air pollutants, and many other extensive areas. Some early works of Chaudhary and Merkin [1-3] had explored the HH reaction in a boundary layer flow. A Survey of the literature reveals the array of investigations on HH chemical reactions. For instance, Suleman et al. [4] investigated the effect of MHD on sliver-water nanofluid over a stretching cylinder. With the consideration of HH reaction, the concentration of the nanomaterial decay with a rise in a chemical reaction with Joule heating. A remarkable impact of HH reaction is recorded and applied to various flow geometries by several researchers. For instance, Ramzan and Naila [5] examined the CNTs stagnation point flow over a stretching surface with HH reaction and Cattaneo-Christov heat flux. The model is tackled numerically using the quasi-linearization technique. Doh et al. [6] also examine the effect of HH reaction on silver-water-based nanofluid over a permeable rotating disk via a semi-analytic method. Their result shows that nanomaterials became less dense with an upsurge in HH reaction. Few related articles are presented in [7-9].

Physically, phenomena such as the thermal radiation effect have significant involvement and varieties of applications such as gas turbines, nuclear power plants. Having this in view, numerous authors have modeled the flow heat and mass transfer of various fluids putting into consideration the effect of thermal radiation. The highlighted survey of the literature shows that the Rosseland approximation used is a linear function of the gradient of radiative heat flux by assuming a small temperature difference within the flow. The three-dimensional flow of Oldroyd B nanofluid over a bidirectional stretching

Corresponding Author**:** Yusuf T.A., Email: tundeayusuf04@gmail.com, Tel: +2348038585662

surface is been examined by Awais et al. [10]. The rheological system under the application of nonlinear thermal radiation and thermophoresis is solved by the use of the homotopy analysis method. Khan et al. [11] explored the steady three-dimensional magnetohydrodynamics (MHD) flow of Powell-Eyring nanofluid with convective and the nanoparticles' mass flux conditions featuring nonlinear thermal radiation. Their report showed that enhanced thermal radiation produces an upsurge in the temperature distribution. Kumar et al. [12] scrutinize the influence of nonlinear thermal radiation over double diffusive free convective boundary layer flow of a viscoelastic nanofluid through a stretching sheet. Recent endeavors in this area can be revealed by the studies [13-15].

It is a tradition to assume the fluid velocity at the wall is the same as the surface, but at a microscopic level, small slips do occur at the fluid-solid juncture as a result of instabilities at high-stress levels in processes like polymer extraction. Slips of such kind affect the motion of the fluid at the surface of the geometry. As reported by Bhattacharyya et al. [16], the assumption of no-slip is rarely applicable for all cases of flow. However, this condition may be replaced with a partial or slip condition. Hamid et al. [17] examined the magnetic effect on stagnation point flow with the influence of slip at the surface using the Crank-Nicolson technique. The fluid velocity is noticed to strengthen for larger slip. Khan et al. [18] studied the partial slip effect of viscous fluid flow over a permeable rotational disk with MHD. The convective flow with slip effect of a non-Newtonian power-law fluid model along with a parallel plate and circular microchannels is studied by Kiyasatfar [19]. The result showed that as the flow speed decelerates and molecular stability elevates against an increase in slip condition. Multiple effects of slip MHD, thermal radiation, and viscous dissipation on the flow of Jeffrey on parallel plates with the porous regime were examined by Ramesh [20]. This report shows that for large slips, the velocity rises while it decayed the temperature profile. Numerous studies that discussed the slip effect under different conditions can be found in [21-24].

The above work of literature survey showed that fewer exploration examining the combined impact of nonlinear thermal radiation and Thompson and Troin slip condition. Presently, no mathematical model has deliberated these effects on a viscous fluid flow over a thin needle. The slip condition Tiwari and Das nanofluid model is adopted here. The generalized slip boundary condition is also integrated into the system, where the length of slip varies with shear stress, as introduced by Thompson and Torian [25] in 1997 and used by Choi et al. [26], Abbas et al. [27] and coined Thompson and Torian slip conditions and the overall model is numerically solved by Runge Kutta Fehlberg method cum shooting technique.

Mathematical analysis

A steady 2-D flow of a viscous fluid over a slippery thin needle with radius $r = R(x)$ is examined. The needle is assumed to be moving with a constant velocity $u_w(x)$ in a free stream where *r* and *x* are the radial and axial coordinates (see Fig. 1). As demonstrated in the diagram, the axial direction *x* is parallel to the moving thin needle, and radial direction *r* is in the direction of the flow that is normal to it. Furthermore, the pressure gradient in the direction of the needle is assumed zero in view of the needle size, however, the impact of the curvature in the transverse direction is important. The fluid is assumed to be electrically conducted with a constant magnetic field B_0 normal to the flow direction. The magnetic Reynolds number is assumed small and so, the induced magnetic field can be considered to be negligible. The Thompson and Torian slip conditions and nonlinear radiative heat transfer effects are taken into consideration.

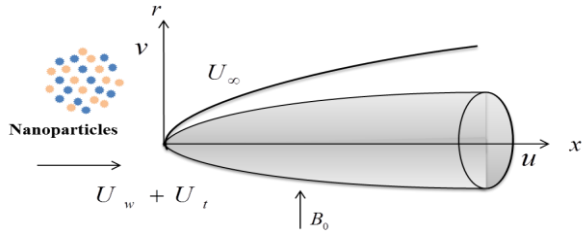

Fig 1: Schematic model for the flow problem

A mathematical relation of the isothermal HH reactions comprising of two chemically reacting species A_c and B_c have been reported by Chaudhary and Merkin [1-2] and Merkin [3] as

$$A_c + 2B_c \to 3B_c, \quad \text{rate} = k_c C_1 C_2^2$$
$$A_c \to B_c, \quad \text{rate} = k_s C_1 \qquad (1)$$

C_1 and C_2 representing the concentrations of the chemical species, rate of constants are k_c and k_s. The mathematical model, in view of the prior assumptions is [28-29]:

$$\frac{\partial}{\partial x}(ru) + \frac{\partial}{\partial r}(rv) = 0, \qquad (2)$$

$$u\frac{\partial u}{\partial x}+v\frac{\partial u}{\partial r}=\frac{\nu}{r}\frac{\partial}{\partial r}\left(r\frac{\partial u}{\partial r}\right)-\frac{\sigma B_0^2 u}{\rho} \tag{3}$$

$$u\frac{\partial T}{\partial x}+v\frac{\partial T}{\partial r}=\frac{\alpha}{r}\frac{\partial}{\partial r}\left(r\frac{\partial T}{\partial r}\right)+\frac{16\sigma_1}{3k^*\left(\rho c_p\right)_f}\left\{T^3\frac{\partial^2 T}{\partial r^2}+3T^2\left(\frac{\partial T}{\partial r}\right)^2\right\}+\frac{\sigma B_0^2 u^2}{\left(\rho c_p\right)_f}+\frac{Q_0\left(T-T_\infty\right)}{\left(\rho c_p\right)_f}$$
$$+\kappa\left[D_B\frac{\partial C_1}{\partial r}\frac{\partial T}{\partial r}+D_B\frac{\partial C_2}{\partial r}\frac{\partial T}{\partial r}+\frac{D_T}{T_\infty}\left(\frac{\partial T}{\partial r}\right)^2\right] \tag{4}$$

$$u\frac{\partial C_1}{\partial x}+v\frac{\partial C_1}{\partial r}=\frac{D_A}{r}\frac{\partial}{\partial r}\left(r\frac{\partial C_1}{\partial r}\right)+\frac{D_T}{T_\infty}\frac{1}{r}\frac{\partial}{\partial r}\left(r\frac{\partial T}{\partial r}\right)-k_c C_1 C_2^2 \tag{5}$$

$$u\frac{\partial C_2}{\partial x}+v\frac{\partial C_2}{\partial r}=\frac{D_B}{r}\frac{\partial}{\partial r}\left(r\frac{\partial C_2}{\partial r}\right)+\frac{D_T}{T_\infty}\frac{1}{r}\frac{\partial}{\partial r}\left(r\frac{\partial T}{\partial r}\right)+k_c C_1 C_2^2 \tag{6}$$

In the above Eqs (2) - (6), velocity components along $x-$ $y-$ and directions are denoted as u and v respectively, T is nanofluid temperature, C_1 and C_2 are the nanofluid concentrations in the boundary layer, respectively, B_0 is the strength of the applied magnetic field, ν is the kinematic viscosity of the fluid, parameter, ρ is the density of the fluid, σ is the fluid electrical conductivity, C_p is the specific heat, α is the fluid thermal diffusivity, σ_1 is the Stephan–Boltzmann constant, k^* is the mean absorption coefficient, D_A and D_B are the diffusion coefficients for chemical species A and B, D_T is the thermophoretic diffusion, k_c and k_s are the rate constant, T_w and T_∞ are the temperature of the surface of the needle and ambient fluid.

The model assumed a generalized slip boundary condition at the surface by Thompson and Troian [25].

Here the tangential velocity U_t is defined as

$$U_t=\lambda_s\left[1-\xi_s\frac{\partial u}{\partial r}\right]^{-\frac{1}{2}}\frac{\partial u}{\partial r} \tag{7}$$

here, λ_s and ξ_s represent the Navier's slip length, and the reciprocal of some critical shear rate.

The model boundary conditions become

$$u=U_w\left(x\right)+U_t=ax+U_t,\ v=0,\ T=T_w, D_A\frac{\partial C_1}{\partial r}=k_s C_1,\quad D_B\frac{\partial C_2}{\partial r}=-k_s C_1,\quad \text{at}\quad r=R\left(x\right)$$
$$u\to U_\infty\left(x\right),\qquad T\to T_\infty,\qquad C_1\to C_0,\qquad C_2\to 0\qquad\qquad \text{as}\quad r\to\infty \tag{8}$$

To convert the governing model to ODEs we define the similarity variables as

$$u=2Uf'\left(\eta\right),\quad v=-\frac{\upsilon_f}{r}f\left(\eta\right)+\eta\frac{\upsilon_f}{r}f'\left(\eta\right),\quad \eta=\frac{Ur^2}{\upsilon_f x},\quad \theta\left(\eta\right)=\frac{\left(T-T_\infty\right)}{\left(T_w-T_\infty\right)},$$
$$G\left(\eta\right)=\frac{C_1}{C_0},\qquad H\left(\eta\right)=\frac{C_2}{C_0} \tag{9}$$

Eq (1) is trivially satisfied, thus, the governing equations are

$$4\left(\eta f''\right)'+2ff''-M^2 f'=0 \tag{10}$$

$$\left(\eta\theta'\right)'+\frac{4}{3}R_T\left\{\begin{matrix}\left[1+\left(T_R-1\right)\theta\right]^3\left(\frac{1}{2}\theta'+\eta\theta''\right)\\ +3\eta\left[1+\left(T_R-1\right)\theta\right]^2\left(T_R-1\right)\left(\theta'\right)^2\end{matrix}\right\}+\Pr\left\{\frac{1}{2}f\theta'+4\eta Ec\left(f''\right)^2\right\}+\frac{Pr}{4}Q\theta$$
$$+\Pr\left\{\eta\left[Nb\left(\theta'G'+\theta'H'\right)+Nt\left(\theta'\right)^2\right]+EcM\left(f'\right)^2\right\}=0 \tag{11}$$

$$\frac{2}{Sc}\left(\eta G'\right)'+f'G'+2\left(\frac{Nt}{Nb}\right)\left(\theta'+\eta\theta''\right)-\frac{1}{2}K_s GH^2=0 \tag{12}$$

$$\frac{2\Omega}{Sc}\left(\eta H'\right)'+f'H'+2\left(\frac{Nt}{Nb}\right)\left(\theta'+\eta\theta''\right)+\frac{1}{2}K_s GH^2=0 \tag{13}$$

By representing the size/thickness of the needle we assume $\eta=A$, the boundary conditions are given as:

$$f'(A)=\frac{1}{2}(1-\delta)+\gamma f''(0)\left[1-\xi f''(0)\right]^{-\frac{1}{2}},\ f(A)=\frac{A}{2}(1-\delta), \tag{14}$$

$$\theta(A)=1,\ G'(A)=K_E G(A),\ \Omega H'(A)=-\frac{1}{2}K_E G(A) \qquad \text{at} \quad \eta=A$$

$$f'(\infty)\to\frac{1}{2}\delta,\quad \theta(\infty)\to 0,\quad G(\infty)\to 1,\quad H(\infty)\to 0 \qquad \text{as} \quad \eta\to\infty \tag{15}$$

Here, M is the magnetic parameter, δ is the ratio parameter, γ is the slip parameter, ξ is the critical shear rate, T_R is the temperature ratio parameter, υ is the kinematic viscosity, Ω is the ratio of diffusion coefficients, $\Pr$ is the Prandtl number, Sc is the Schmidt number, R_T is the radiation parameter, N_t is the thermophoresis parameter, λ is the ratio parameter, K_s, K_E and Ω are the intensity of homogeneous-heterogeneous reaction parameters, Ec is the Eckert number and Q is the heat source parameter.

The dimensionless form of these parameters are defined as

$$\delta=\frac{U_w}{U},T_R=\frac{T_w}{T_\infty},\ \Pr=\frac{\nu}{\alpha},R_T=\frac{4\sigma_1 T_\infty^3}{k^* k},K_S=\frac{k_c C_0^2 x}{U},M=\frac{\sigma B_0^2 x}{\rho U},\ K_E=\frac{k_s \upsilon x}{D_A U r},Sc=\frac{\upsilon}{D}, \tag{16}$$

$$Nb=\frac{\kappa D_B C_0}{\upsilon},\ Q=\frac{Q_0 x}{\rho C_p U},\ \Omega=\frac{D_B}{D_A},\quad Nt=\frac{\kappa D_T T_\infty (T_R-1)}{\upsilon T_\infty},\ E_c=\frac{U^2}{(c_p)_f (T_R-1)T_\infty}$$

Oftentimes, the diffusion coefficient of chemical species A_c and B_c is of comparable size. We, therefore, assume that the diffusion coefficients D_A and D_B are identical, i.e., Ω=1.

$$H(\eta)+G(\eta)=1 \tag{17}$$

With the above equation, Eqs (11) - (13) with the corresponding boundary condition yield

$$(\eta\theta')'+\frac{4}{3}R_T\left\{\begin{matrix}\left[1+(T_R-1)\theta\right]^3\left(\frac{1}{2}\theta'+\eta\theta''\right)\\ +3\eta\left[1+(T_R-1)\theta\right]^2(T_R-1)(\theta')^2\end{matrix}\right\}+\Pr\left\{\frac{1}{2}f\theta'+4\eta Ec(f'')^2\right\} \tag{18}$$

$$+\frac{\Pr}{4}Q\theta+\Pr\left\{\eta Nt(\theta')^2+EcM^2(f')^2\right\}=0$$

$$\frac{2}{Sc}(\eta G''+G')+f'G'+2\left(\frac{Nt}{Nb}\right)(\theta'+\eta\theta'')-\frac{1}{2}K_S G(1-G)^2=0 \tag{19}$$

$$G'(A)=\frac{1}{2}K_E G(A),\qquad G(\infty)\to 1$$

The skin friction and the Nusselt number are given as

$$\left.\begin{matrix}C_f=\frac{\mu}{\rho U^2}\left(\frac{\partial u}{\partial r}\right)_{r=A},\\ Nu_x=-\frac{x}{(T_w-T_\infty)}k\left(1+\left(\frac{16\sigma_1 T_\infty^3}{3k^* k}\right)\right)\left(\frac{\partial T}{\partial r}\right)_{r=A}\end{matrix}\right\} \tag{20}$$

the dimensionless form are

$$\left.\begin{matrix}\mathrm{Re}_x^{0.5}C_f=4\sqrt{A}f''(A),\\ \mathrm{Re}_x^{-0.5}\,\mathrm{Nu}=-2\sqrt{A}\left[1+\frac{4}{3}R_T\left\{\theta(A)(T_R-1)+1\right\}^3\right]\theta'(A),\end{matrix}\right\} \tag{21}$$

Solution technique

The result of the nonlinear system (10), (17-18) subject to (14) is computed numerically by the Runge-Kutta Fehlberg method cum shooting technique. In this numerical scheme, 0.001 and 10^{-6} were taken as the step size and convergence criteria respectively. A finite value for the far boundary condition $(\eta\to\infty)$ in Eqn (14) is also taken as $\eta_{\max}=20$. This technique has remained extremely popular and maintained comparable efficiency to other numerical methods, such as finite elements and spectral methods. This method is well-orthodox in the reports and therefore details are not publicizing here. For details, readers can refer to Mabood et al. [29]. The below values of parameters are used throughout the computation unless otherwise mentioned.

Result and Discussion

For clarity and understanding, the computed solutions of the mathematical dimensionless formulation are graphically illustrated for the entrenched parameter sensitivity. Various parameter reliant results for the flow characteristics and technology quantities of concern (i.e. velocity $f'(\eta)$, temperature $\theta(\eta)$, concentration $G(\eta)$, skin friction coefficient, and the Nusselt number) are confirmed. The ranges of value adopted for this study are found on the value associated with theoretical and experimental analysis reported in different articles. To establish the correctness of the used numerical method, computed results assessment is presented in Table 1. The results comparison with recent related studies by [28, 29] shows a good quantitative agreement with the present one as shown in Table 1.

The sensitivity of conducting reactive flowing nanofluid in a thin needle to variation in the slip parameter (γ) and magnetic term (M) is established in Figure 2. As seen, increasing the needle stretching slip simulates heat around the thin wall that decreases the nanoparticles' bonding strength. Both the reaction and nanoparticles collision within the thin needle is thereby energized. Hence, the flowing fluid velocity rises as the slip term is increased as observed in Figure 2a. However, contrast flow behavior is noticed in Figure 2b for a rising magnetic term. As the values of the parameter (M) enhanced, an opposing force is induced in a nanofluid reaction that dragged the flow rate. The parameter influence is very significant due to the combined effect of Lorentz force and thinning flow medium. As such, the collective nanofluid reactions in the device decelerate at little variation in the parameter as depicted in Figure 2b.

In Figure 3, the response of the non-Newtonian flowing nanofluid velocity to varying in the needle thickness/size (A) and the velocity ratio parameter (δ) is revealed. As found in Figure 3a, enhancing the needle thickness boosts the narrowness of the needle medium thereby increases the fluid friction and viscosity. As a result, the flow resistance forces are encouraged which leads to dragging of the motion of the nanoparticle, as such, the flow magnitude is reduced progressively towards the far steam. Meanwhile, the nanofluid flow rate in the thin needle medium rises momentously with the steady rise in the velocity stretching ratio as displayed in Figure 3b. Close to the slipping wall at the early stage of the reactions, the velocity of the flowing fluid reduces due to the dominance of heterogeneous reactions. However, a short distance away from the stretching wall along the flow stream, the velocity of the nanofluid upsurges remarkably with a slight rise in the parameter values. The homogenous chemical reaction controlled the fluid reactions which later revised the flow behavior as offered in Figure 3b. Therefore, the flow momentum is augmented as heat is generated in the device.

Figures 4, 5 and 6 show the parametric sensitivity justification and confirmation of the nanofluid thermal conduction and distributions in a thin needle with heterogeneous and homogenous reactions. The chemical reaction nanofluid heat dispersion under the influence slip term (γ) is obtained in Figure 4a. The slip velocity discourages internal heat formation terms in the temperature equation which leads to a decrease in the nanoparticles heat transfer. Figure 4b denotes the impact of magnetic terms on the heat transport system. The conducting nanofluid dragged in the flow medium due to rise bonding strength and increasing fluid viscosity that enhances internal energy generation. This then inspired heat transfer that raises the temperature profile as illustrated in Figure 4b. In Figure 5, the responses of reactive nanofluid temperature distribution to variation in the radiation term (R_T) and temperature ratio (T_R) are described. Both parameters encourage nanoparticle thermal conductivity by increases energy transport that causes a rise in the temperature profiles. As noticed, the thin needle device boundary surface thickness is augmented which dampens heat dispersion to the ambient, as such, the heat within the system is enhanced. As a result of continuous heat production due to active homogenous reaction species, the nanofluid heat conduction and transfer are improved that in turn raises the overall temperature field along the flow region. The effect of increasing the needle thickness (A) and Eckert number (Ec) on the nanofluid temperature distribution in a thin needle is shown in Figure 6. A noteworthy increment in the heat generation is observed that completely boosts the heat field and reduces the fluid viscosity. Also, the parameters strengthen the boundary surface thickness and heat source that boosts the temperature profiles.

The plot of species concentration $G(\eta)$ against the flow distance (η) for various effects of dependent parameters on the conducting nanofluid in a thin needle is established in Figures 7 to 11. In Figure 7, the device wall slip velocity and magnetic term influence on the species concentration is obtained. The velocity slip term increases the concentration profile by stimulating heat energy that is propagated by the nanoparticles to support the chemical reaction. As seen, the heterogeneous and homogeneous chemical reaction is propelled that in turn raises the species distribution. Meanwhile, the magnetic term diminishes the species mass profile by stirring the reactive fluid viscosity that strengthening the molecular bonding force. Hence, the species reaction rate of the considered fluid concentration is opposed and this resulted in concentration magnitude reductions. The sensitivity of the concentration diffusion to changes in the radiation term and temperature ratio respectively reported in Figures 8a and 8b. The species mass profile reduces due to insufficient internal heat generation to induce the reaction process as the parameters (R_T) and (T_R) vary. The fluid friction is enhanced to resist

molecular diffusion, thus weakens nanofluid species reaction. More so, the species concentration reaction distribution in the thin needle medium decreases completely throughout the flow regime.

The response of species molecular mass to rising values of heterogeneous reaction term (K_E) and thermophoresis (N_t) is confirmed in Figure 9. In Figure 9a, an increase in the heterogeneous reaction breaks the nanofluid molecular reactants into different phases thereby reduces the overall system reaction rate. Hence, the concentration distribution is declining. Similarly, in Figure 9b, the thermophoresis parameter decreases the molecular species mixture due to different responses by the mobile nanoparticles to a temperature gradient force. As such, the species mass transfer reduces the weak response of the nanoparticles to gradient force. The Schmidt number (Sc) and chemical reaction (K_s) effects on the reaction concentration profile are verified in Figure 10. The Schmidt number defines the kinematic viscosity ratio to mass diffusion. It is observed that the nanofluid experienced concurrent mass and momentum diffusion convective process, this reduces the fluid viscosity. As a result, there is strong molecular diffusion in the thin needle that leads to a rise in mass transfer. However, the chemical reaction term declines the species molecular transport by enhancing the nanofluid viscosity in the medium as obtained in Figure 10b. Figure 11 shows the influence of needle thickness and Eckert number on the species distribution. Both terms significantly decrease the concentration profiles. The resulted flow behavior is due to a strong molecular species bonding force caused by low nanoparticles thermal conduction and the dominance of heterogeneous reaction. High heat dissipation to the surroundings occurs through the needle wall thereby reduces the heat within the system, as such, the nanofluid reactive mixture mass transfer diminished.

The plot of C_f against (δ) demonstrating the wall shear stress for variation in the magnetic parameter (M), slip velocity (γ) and Navier slip term (ξ) is presented in Figure 12. The wall skin friction decreases for all the considered dependent parameters due to a thinner momentum wall surface. The wall dragging force is damped as the parameter values rise. Also, as noticed in Figures 13a and 13c, the Nusselt effect reduces as the magnetic and Navier slips terms increase due to large diffusion of heat as the reaction mixture encourages wall thermal conductivity which enables heat transfer at the needle boundary surface. But the opposite response is noticed in Figure 13b for an increasing radiation term that causes a rise in the heat gradient at the wall. The rising heat gradient is because the thermal boundary layer is boosted as the thermal radiation varies.

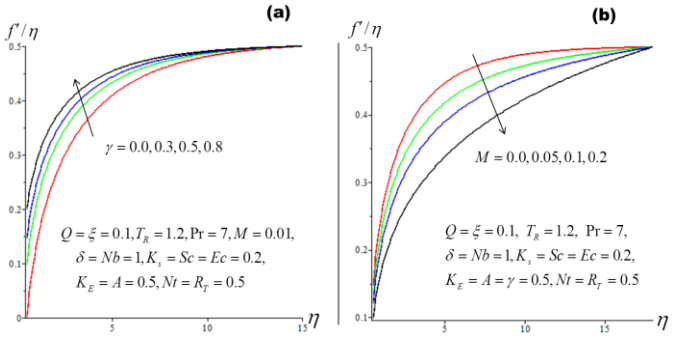

Fig 2: Impact of γ and M on $f'(\eta)$

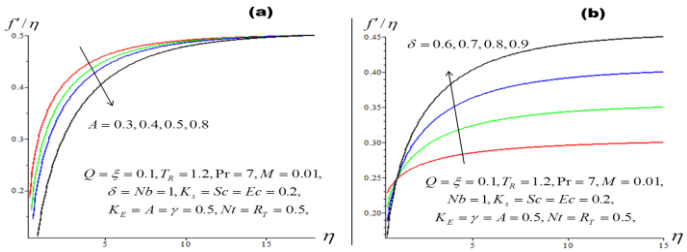

Fig 3: Impact of A and δ on $f'(\eta)$

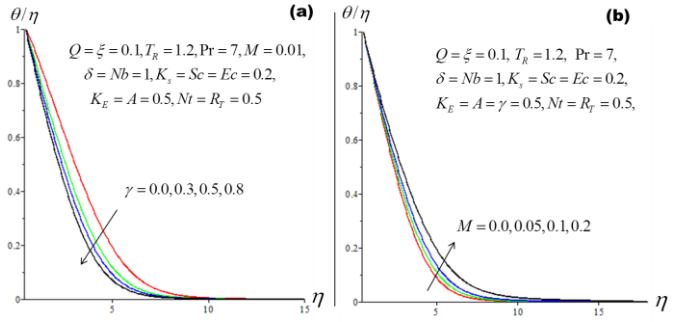

Fig 4: Impact of γ and M on $\theta(\eta)$

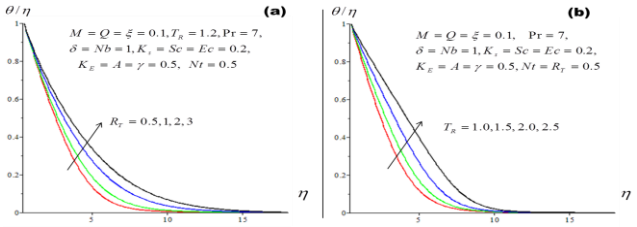

Fig 5: Impact of R_T and T_R on $\theta(\eta)$

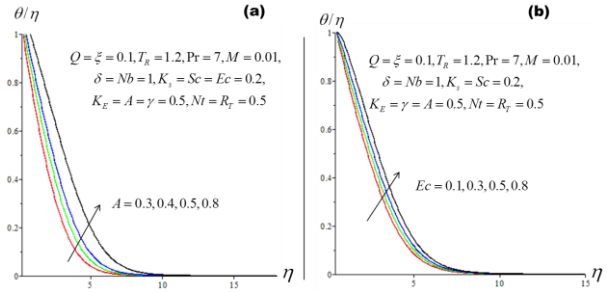

Fig 6: Impact of A and Ec on $\theta(\eta)$

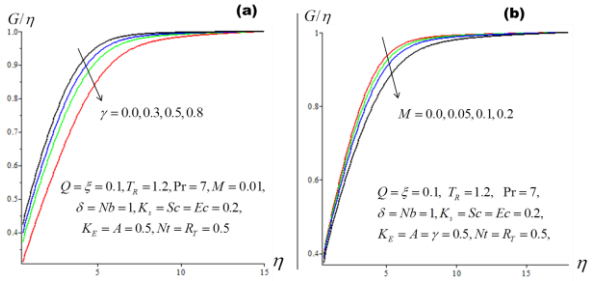

Fig 7: Impact of γ and M on $G(\eta)$

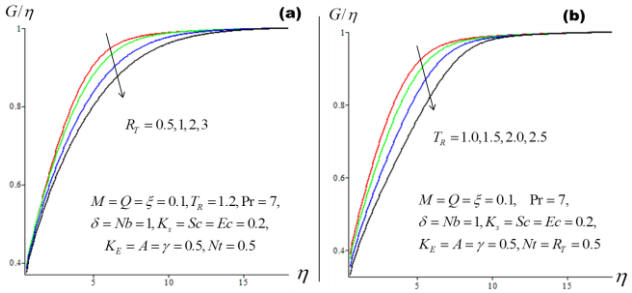

Fig 8: Impact of R_T and T_R on $G(\eta)$

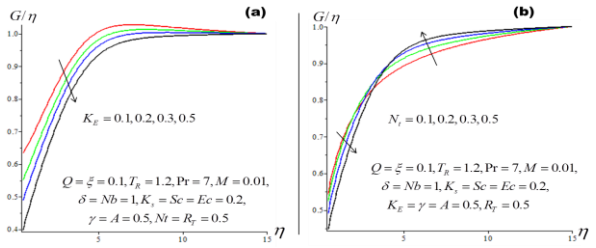

Fig 9: Impact of K_E and N_t on $G(\eta)$

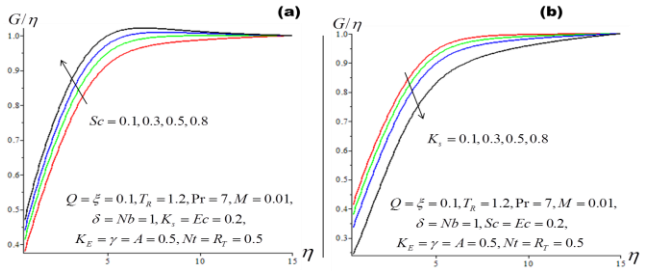

Fig 10: Impact of Sc and K_s on $G(\eta)$

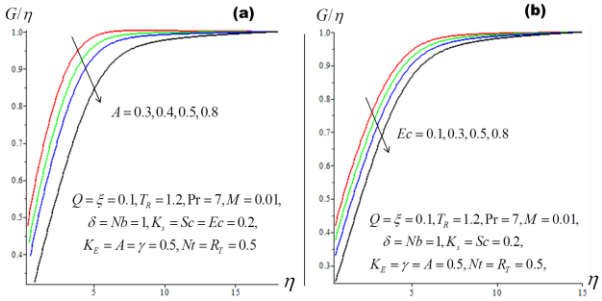

Fig 11: Impact of A and Ec on $G(\eta)$

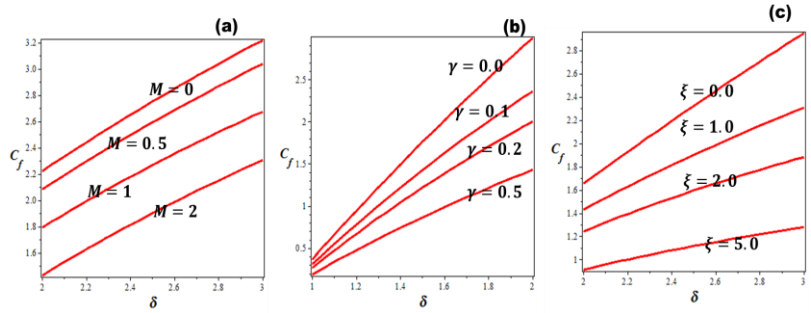

Fig 12: Fig 12: Impact of M, γ and ξ on skin friction coefficient

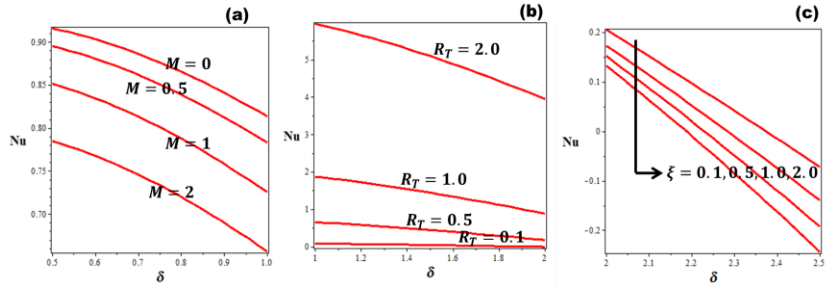

Fig 13: Impact of M, R_T and ξ on Nusselt number

Table 1: Comparision of values of skin friction with the previous result for $M = \lambda = \xi = 0$

A	δ	Salleh et al. [28]	Mabood et al. [29]	Present result
0.01	0.0	8.492445	-	8.4924453
0.01	0.7	-	2.662170	2.6621693
0.01	1.0	-	6.79297	6.7929721
0.15	0.0	0.938339	-	0.9383388
0.2	0.0	0.751572	-	0.7515724
0.2	0.7	-	1.10033	1.1003253

Conclusion

In the present investigation, the numerical aspect of the nonlinear thermal radiative flow of a nanofluid in the presence of a magnetic field over a thin needle is examined. The study adopted a flow model with Thompson and Troian slip condition for the heat and mass transfer of homogeneous-heterogeneous reactions. Some significant outcomes of the current studies are highlighted below:

i. The chemical reaction flow transitional regime is increased with the rising non-Newtonian material property.
ii. The homogeneous-heterogeneous chemical reaction arouses the fluid material viscosity that leads to concentration damping.
iii. Radiation and temperature ratio greatly influence the heat transfer by reducing the fluid viscosity and support the dominance of homogeneous reactions in the system.
iv. The temperature gradient and shear stress magnitude at the thin needle wall decreases for rising values of M, γ, ξ but the heat gradient quantity reverses for increasing values of R_T.
v. Heterogeneous chemical reaction and thermophoresis parameters significantly reduce the nanofluid molecular species transfer.

The observations and results of this study have motivating applications and implications for the engineering, industrial, and mathematical solutions analysis of nanofluid flow in a thin needle with a homogeneous-heterogeneous reaction. The study can be extended to the horizontal complex flows in the annuli cylinder.

Reference

[1] M.A. Chaudhary, J.H. Merkin, Homogeneous-heterogeneous reactions in boundary-layer flow: Effects of loss of reactant, Mathematical and Computer Modeling, 24 (1996) 21-8.
[2] M.A. Chaudhary, J.H. Merkin, A simple isothermal model for homogeneous-heterogeneous reactions in boundary layer flow: I. equal diffusivities, Fluid Dynamics Research. 16 (1995) 311–333.
[3] J.H. Merkin, A model for isothermal homogeneous-heterogeneous reactions in boundary-layer flow, Mathematical and Computer Modeling, 24 (1996) 125-36.
[4] M. Suleman, M. Ramzan, S. Ahmad, D. Lu, Numerical simulation for homogeneous– heterogeneous reactions and Newtonian heating in the silver-water nanofluid flow past a nonlinear stretched cylinder. Physica Scripta, 94(8) (2019) 085702.
[5] M. Ramzan, N. Shaheen, Thermally stratified Darcy–Forchheimer nanofluid flow comprising carbon nanotubes with effects of Cattaneo–Christov heat flux and homogeneous–heterogeneous reactions. Physica Scripta, 95(1) (2019) 015701.
[6] D. H. Doh, M. Muthtamilselvan, B. Swathene, E. Ramya, Homogeneous and heterogeneous reactions in a nanofluid flow due to a rotating disk of variable thickness using HAM. Mathematics and Computers in Simulation, 168 (2020) 90-110.
[7] I. Khan, M. Y. Malik, A. Hussain, T. Salahuddin, Effect of homogenous-heterogeneous reactions on MHD Prandtl fluid flow over a stretching sheet. Results in physics, 7 (2017) 4226-4231.
[8] M. Ramzan, N. Shaheen, Thermally stratified Darcy–Forchheimer nanofluid flow comprising carbon nanotubes with effects of Cattaneo–Christov heat flux and homogeneous–heterogeneous reactions. Physica Scripta, 95(1) (2019) 015701.
[9] M. Imtiaz, F. Mabood, T. Hayat, A. Alsaedi, Homogeneous-heterogeneous reactions in MHD radiative flow of second grade fluid due to a curved stretching surface. International Journal of Heat and Mass Transfer, 145 (2019) 118781.
[10] M. Awais, T. Hayat, N. Muqaddass, A. Ali, Aqsa, Saeed Ehsan Awan, Nanoparticles and nonlinear thermal radiation properties in the rheology of polymeric material, Results in Physics 8 (2018) 1038–1045.
[11] M. Khan, M. Irfan, W.A. Khan, L. Ahmad, Modeling and simulation for 3D magneto Eyring–Powell nanomaterial subject to nonlinear thermal radiation and convective heating, Results in Physics 7 (2017) 1899–1906

[12] Kumar KG, Gireesha BJ, Manjunatha S, Rudraswamy NG. Effect of nonlinear thermal radiation on double-diffusive mixed convection boundary layer flow of viscoelastic nanofluid over a stretching sheet. Int J Mechan Mater Eng. 2017;12(2017):1–18

[13] Pantokratoras A. Natural convection along a vertical isothermal plate with linear and nonlinear Rosseland thermal radiation. Int J Therm Sci 2014; 84:151–7.

[14] Mushtaq A, Mustafa M, Hayat T, Alsaedi A. On the numerical solution of the nonlinear radiation heat transfer problem in a three-dimensional flow. Z Naturforsch 2014; 69:705–13.

[15] B.C. Prasannakumara, B.J. Gireesha, M.R. Krishnamurthy, K. Ganesh Kumar, MHD flow and nonlinear radiative heat transfer of Sisko nanofluid over a nonlinear stretching sheet, Informatics in Medicine Unlocked 9 (2017) 123–132

[16] G. C. Bhattacharyya, K. Mukhopadhyay and S. Layek 2011 Slip effects on boundary layer stagnation-point flow and heat transfer towards a shrinking sheet Int. J. Heat Mass Transf. 54(1–3) 308–313

[17] M. Hamid, T. Zubair, M. Usman, Z. H. Khan, W. Wang, Natural convection effects on heat and mass transfer of slip flow of time-dependent Prandtl fluid. Journal of Computational Design and Engineering (2019)

[18] M. I. Khan, T. Hayat, M. I. Khan, M. Waqas, A. Alsaedi, Numerical simulation of hydromagnetic mixed convective radiative slip flow with variable fluid properties: a mathematical model for entropy generation. Journal of Physics and Chemistry of Solids, 125 (2019) 153-164.

[19] M. Kiyasatfar, Convective heat transfer and entropy generation analysis of non-Newtonian power-law fluid flows in parallel-plate and circular microchannels under slip boundary conditions. International Journal of Thermal Sciences, 128 (2018) 15-27.

[20] K. Ramesh, Effects of viscous dissipation and Joule heating on the Couette and Poiseuille flows of a Jeffrey fluid with slip boundary conditions. Propulsion and Power Research, 7(4) (2018) 329-341.

[21] S. E. Ahmed, M. A. Mansour, A. Mahdy, S. S. Mohamed, Entropy generation due to double diffusive convective flow of Casson fluids over nonlinearity stretching sheets with slip conditions. Engineering Science and Technology, an International Journal, 20(6) (2017) 1553-1562.

[22] M. Shojaeian, A. Koşar, Convective heat transfer and entropy generation analysis on Newtonian and non-Newtonian fluid flows between parallel-plates under slip boundary conditions. International Journal of Heat and Mass Transfer, 70 (2014) 664-673.

[23] G. G. Pereira, Effect of variable slip boundary conditions on flows of pressure driven non-Newtonian fluids. Journal of Non-Newtonian Fluid Mechanics, 157(3) (2009) 197 - 206

[24] S. R. R. Reddy, P. B. A. Reddy, K. Bhattacharyya, Effect of nonlinear thermal radiation on 3D magneto slip flow of Eyring-Powell nanofluid flow over a slendering sheet with binary chemical reaction and Arrhenius activation energy. Advanced Powder Technology, 30(12) (2019) 3203-3213.

[25] P. A. Thompson, S. M. Troian, A general boundary condition for liquid flow at solid surfaces. Nature, 389(6649) (1997) 360.

[26] C. H. Choi, K. J. A. Westin, K. S. Breuer, Apparent slip flows in hydrophilic and hydrophobic microchannels. Physics of fluids, 15(10) (2003) 2897-2902.

[27] Z. Abbas, M. Sheikh, J. Hasnain, H. Ayaz, A. Nadeem, Numerical aspects of Thomson and Troian boundary condition in Tiwari-Das nanofluid model with homogeneous-heterogeneous reactions. Physica Scripta (2019).

[28] S. N. A Salleh , N. Bachok, N. Md Arifin & F. Md Ali, Numerical analysis of boundary layer flow adjacent to a thin needle in nanofluid with the presence of heat source and chemical reaction, Symmetry, 2019, *11*, 543; doi:10.3390/sym11040543

[29] F Mabood, M.K. Nayak, & A J. Chamkha, Heat transfer on the cross flow of micropolar fluids over a thin needle moving in a parallel stream influenced by binary chemical reaction and Arrhenius activation energy, Eur. Phys. J. Plus (2019) 134: 427, DOI 10.1140/epjp/i2019-12716-9